The Astronomical Journal, 166:95 (15pp), 2023 September https://doi.org/10.3847/1538-3881/ace111


# Variability in NGC 3201 Giant Stars

C. C. Cortés[1], Á. Llancaqueo Albornoz[2], S. Villanova[2], J. A. Ahumada[3], and C. Parisi[3,4]
[1] Departamento de Tecnologías Industriales, Faculty of Engineering, Universidad de Talca, Merced 437, Curicó, Chile; caddy.cortes@utalca.cl
[2] Departamento de Astronomía, Casilla 160-C, Universidad de Concepción, Concepción, Chile
[3] Observatorio Astronómico, Universidad Nacional de Córdoba, Laprida 854, 5000, Córdoba, Argentina
[4] Instituto de Astronomía Teórica y Experimental (CONICET-UNC), Laprida 854, 5000, Córdoba, Argentina
*Received 2023 April 6; revised 2023 June 12; accepted 2023 June 13; published 2023 August 7*

## Abstract

We present the analysis of 510 light curves in $V$ and $I$ bands of 255 giant stars in the globular cluster NGC 3201. Our aim is to expand the sample of new types of variables reported in a previous study. These variables show a short period ($P_V < 0.6$ day) and a low amplitude ($A(V) < 0.06$ mag.). We first searched for variability using the generalized Lomb–Scargle and phase dispersion minimization periodograms of the sample, discarding 167 stars as non-variables. We then applied the significance test and reduced the sample to 88 giants, of which we classified 18 as possible variables, 11 as dubious, 41 as non-variables, and 18 as variables. We finally determined the cluster membership of this sample and grouped each star based on their light-curve shape. The discovered variables show periods in the range $0.2440 < P_V < 0.5868$ days and amplitudes between $0.010 < A(V) < 0.064$ mag. Within the sample of 18 variable stars, we report the discovery of an object with a period $P_V = 0.3603 \pm 0.0012$ and amplitude $A(V) = 0.703 \pm 0.029$ mag that shows a RR Lyrae ab-type light curve. Additionally, we report two RR Lyrae ab and c types with ultralow amplitude.

*Unified Astronomy Thesaurus concepts:* Globular star clusters (656); Variable stars (1761)

*Supporting material:* machine-readable tables

## 1. Introduction

The study of Globular Clusters (GCs) provides huge contributions to the knowledge of our Galaxy because they are the oldest objects and witnesses of the formation of the Milky Way. At first, these objects were assumed to be an example of single stellar populations. However, these claims were disproven by studies such as Gratton et al. (2004) and Carretta et al. (2009a, 2009b), who provided deep and detailed chemical analyses of stars in GCs, and showed that almost all GCs (with the sole exception to date of Ruprecht 106, Villanova et al. 2013) present inhomogeneities in their light element content, with the Na-O anticorrelation being the most distinguishable feature. In addition, the study of galactic GCs is fundamental because it provides knowledge about the halo and bulge of the Milky Way by analyzing their kinematics and dynamics properties.

Among these objects, an interesting case is the low galactic latitude GC NGC 3201 (C1015−461) ($l = 277.^{\circ}23$, $b = +8.^{\circ}64$), which is located at $\alpha = 10^{h}17^{m}36.^{s}82$, $\delta = -46^{\circ}24'44.''9$ (J2000) (Harris 1996, 2010 edition) at a distance of ∼4.9 kpc. This GC has been the object of several studies, such as the debate about the presence of an intrinsic iron spread (e.g., Gonzalez & Wallerstein 1998; Muñoz et al. 2013; Simmerer et al. 2013; Mucciarelli et al. 2015, and references therein) based on high-resolution spectra from instruments such as the UVES-FLAMES@VLT and MIKE@Magellan, as well as works regarding its variable star population (e.g., Layden & Sarajedini 2003; Arellano Ferro et al. 2014; Kaluzny et al. 2016). In fact, this GC is known for its rich content in variable stars, with a list of 121 targets according to the 2012 update of the Catalogue of Variable Stars in Globular Clusters (CVSGC; Clement et al. 2001), containing RR Lyrae, SX Phoenicis, eclipsing binaries, and so on.[5]

It is worth noting that Layden & Sarajedini (2003) showed that NGC 3201 contains several red giant branch (RGB) stars with low-amplitude variations. This happens because RGB stars are unstable against radial pulsations because they evolve through expansion and cooling during the RG or asymptotic giant branch (AGB) stages. Moreover, we know about the existence of pulsating red giants, which present low amplitudes and large periods. A general classification for these objects can be found in the series of papers from Olin Eggen (e.g., Eggen 1973, 1977).

When we move to the metallicity determination, a first clue about a possible relation between variability and iron abundance in red giants as measured by high-resolution spectra is presented in Muñoz et al. (2018), who performed a chemical abundance analysis of seven stars of NGC 6528 using data from the VVV survey (Minniti et al. 2010; Saito et al. 2012). The authors found that one of the RGB stars of the sample is a variable with a period of 0.26 day and an infrared amplitude of 0.05 mag. It is also more metal-poor—[Fe/H] = −0.55—than the other six stars (which have [Fe/H] = −0.14 ± 0.03 on average). Based on this finding, Albornoz et al. (2021) analyzed 17 stars in NGC 3201 that were studied spectroscopically in Simmerer et al. (2013) and Mucciarelli et al. (2015), and reported that stars presenting variable behavior have a larger spread in iron abundances, while non-variable stars show iron abundances close to the mean value of the cluster, thus providing evidence that variability can be a possible explanation for the iron spread suggested by some authors.

In this paper we continue the work by Albornoz et al. (2021) and analyze 510 light curves (LCs) of 255 giant stars—255 in



[5] http://www.astro.utoronto.ca/~cclement/read.html

$V$ and 255 in $I$—of the globular cluster NGC 3201. This time, we solely focus on determining the possible variability of each star within the limitations of our data by performing extensive analysis for each LC. In Section 2 we present the information regarding the data that we used in the work. Section 3 provides details of the methodology that we used to analyze the sample. Section 4 contains the main results obtained from this analysis. Finally, in Section 5 we summarize the results and give the conclusions.

## 2. The Data

We analyzed 255 LCs of giant stars from NGC 3201 in the $V$ and $I$ bands to carry out this research. The giant stars were selected by means of the magnitude color diagram. The data, provided by J. Ahumada and originally published by Arellano Ferro et al. (2014), were obtained on 2013 March 20–23 at the Complejo Astronómico El Leoncito (CASLEO), San Juan, Argentina, using the 2.15 m telescope, and consist of $V$ and $I$ observations. The detector used was a Roper Scientific back-illuminated CCD of $2048 \times 2048$ pixels with a $0\farcs15\,\mathrm{pix}^{-1}$ scale and a field of view of approximately $5.1 \times 5.1$ arcmin$^2$.

The details regarding data reduction and transformation to the $VI$ standard magnitude system are described in Sections 2.2 and 2.3 of Arellano Ferro et al. (2014). We will summarize the data reduction process, which was made with the DanDIA[6] pipeline (Bramich et al. 2013). This pipeline models the convolution kernel that matches the PSF of a pair of images of the same field as a discrete pixels array (Bramich 2008). The details about the DanDIA pipeline are available in the article by Bramich et al. (2011). Additionally, due to the error in the fitted value of the photometric scale factor corresponding to each image, a magnitude offset may be introduced into the photometry, which was resolved using the methodology described by Bramich & Freudling (2012). To transform the instrumental system into the Johnson-Kron-Cousins photometric system (Landolt 1992), we used 85 standard stars of Stetson (2000)[7] that were identified in the field of view of our images. The transformation equations are as follows:

$$V = v + 0.0440(\pm 0.0076)(v - i) - 1.2353(\pm 0.0054)$$

$$I = i + 0.0190(\pm 0.0089)(v - i) - 1.7821(\pm 0.0064).$$

Table 1 shows the content of the LC file data of each star that was analyzed in this work. Each file contained on average more than 140 epochs (with a few exceptions that contain less than 100 epochs), which spans the four nights of observation mentioned previously.

**Table 1**
Sample Time Series for $V$ and $I$ Filters of Each Star

| Star | Filter | HJD (d) | $M_{\rm std}$ (mag) | $\sigma_{M_{\rm std}}$ (mag) | $\sigma_{\rm int}$ (mag) |
|---|---|---|---|---|---|
| N° 1 | $V$ | 2456371.522859 | 15.36361 | 0.0075 | 0.00074 |
| N° 1 | $V$ | 2456371.525984 | 15.35902 | 0.0074 | 0.00063 |
| ⋮ | ⋮ | ⋮ | ⋮ | ⋮ | ⋮ |
| N° 1 | $V$ | 2456374.785581 | 15.35882 | 0.0075 | 0.00125 |
| N° 1 | $V$ | 2456374.789264 | 15.35902 | 0.0075 | 0.00128 |
| N° 1 | $I$ | 2456371.517222 | 14.11365 | 0.0088 | 0.00199 |
| N° 1 | $I$ | 2456371.519717 | 14.11083 | 0.0088 | 0.00181 |
| ⋮ | ⋮ | ⋮ | ⋮ | ⋮ | ⋮ |
| N° 2 | $V$ | 2456371.522859 | 14.53697 | 0.0.0076 | 0.00114 |
| N° 2 | $V$ | 2456371.525984 | 14.53542 | 0.0.0075 | 0.00096 |
| ⋮ | ⋮ | ⋮ | ⋮ | ⋮ | ⋮ |
| N° 2 | $I$ | 2456371.517222 | 13.27920 | 0.0.0088 | 0.00129 |
| N° 2 | $I$ | 2456371.519717 | 13.28237 | 0.0.0089 | 0.00119 |
| ⋮ | ⋮ | ⋮ | ⋮ | ⋮ | ⋮ |
| N° 88 | $V$ | 2456371.522859 | 15.57376 | 0.0.0057 | 0.00201 |
| N° 88 | $V$ | 2456371.525984 | 15.59121 | 0.0.0056 | 0.00180 |
| ⋮ | ⋮ | ⋮ | ⋮ | ⋮ | ⋮ |
| N° 88 | $V$ | 2456374.785581 | 15.54749 | 0.0057 | 0.00154 |
| N° 88 | $V$ | 2456374.789264 | 15.54976 | 0.0057 | 0.00158 |
| N° 88 | $I$ | 2456371.517222 | 15.28730 | 0.0067 | 0.00485 |
| N° 88 | $I$ | 2456371.519717 | 15.27260 | 0.0066 | 0.00418 |
| ⋮ | ⋮ | ⋮ | ⋮ | ⋮ | ⋮ |

(This table is available in its entirety in machine-readable form.)

## 3. Search for Variability and Analysis of the Light Curves

In this section, we first describe the methodology used to search for this new type of variable star. We then explain the statistical analysis that allows us to discard possible false positives. This is the same procedure that was carried out in Section 3 from Albornoz et al. (2021).

### 3.1. Search for Variable Stars

To search for this type of variable star, i.e., with a short period and low amplitude, we applied both the generalized Lomb–Scargle (GLS, Zechmeister & Kürster 2009)[8] and the phase dispersion minimization (PDM, Stellingwerf 1978)[9] periodograms using the PyAstronomy[10] (PyA) package collection (Czesla et al. 2019) in *Python*. We use a GLS periodogram because it is optimized to identify a periodic signal in a sinusoidal shape in the time series. This method produces more precise frequencies, is less affected by overlap, and provides better intensity determination than the Lomb–Scargle algorithm (Lomb 1976; Scargle 1982). Additionally, we complement this method with the PDM periodogram, which uses a test period, and then divides the time series into bins and calculates the variance of the amplitude within each bin. The bin variance is combined and compared to the overall variance of the data set. A true period can be found when the ratio of the bin variance to the total is small. This is the reason why a difference can be noticed between the two periods (see Figure 1). Therefore, we used PDM and complement it with GLS because it is helpful for non-sinusoidal variations of data sets with few irregularly spaced observations, which fits our data.

We complement the period search through PDM from the Image Reduction and Analysis Facility (IRAF; Tody 1986) package because PDM from the PyAstronomy package works using equidistant bins to group the data, while PDM from IRAF requires the us to define the resolution of the theta plot to be used in the period range that we established. The advantage that the PDM from IRAF provides is that it has more direct

[6] http://www.danidl.co.uk/
[7] https://www.canfar.net/storage/list/STETSON/Standards
[8] https://pyastronomy.readthedocs.io/en/latest/pyTimingDoc/pyPeriodDoc/gls.html
[9] https://pyastronomy.readthedocs.io/en/latest/pyTimingDoc/pyPDMDoc/classes.html
[10] https://github.com/sczesla/PyAstronomy

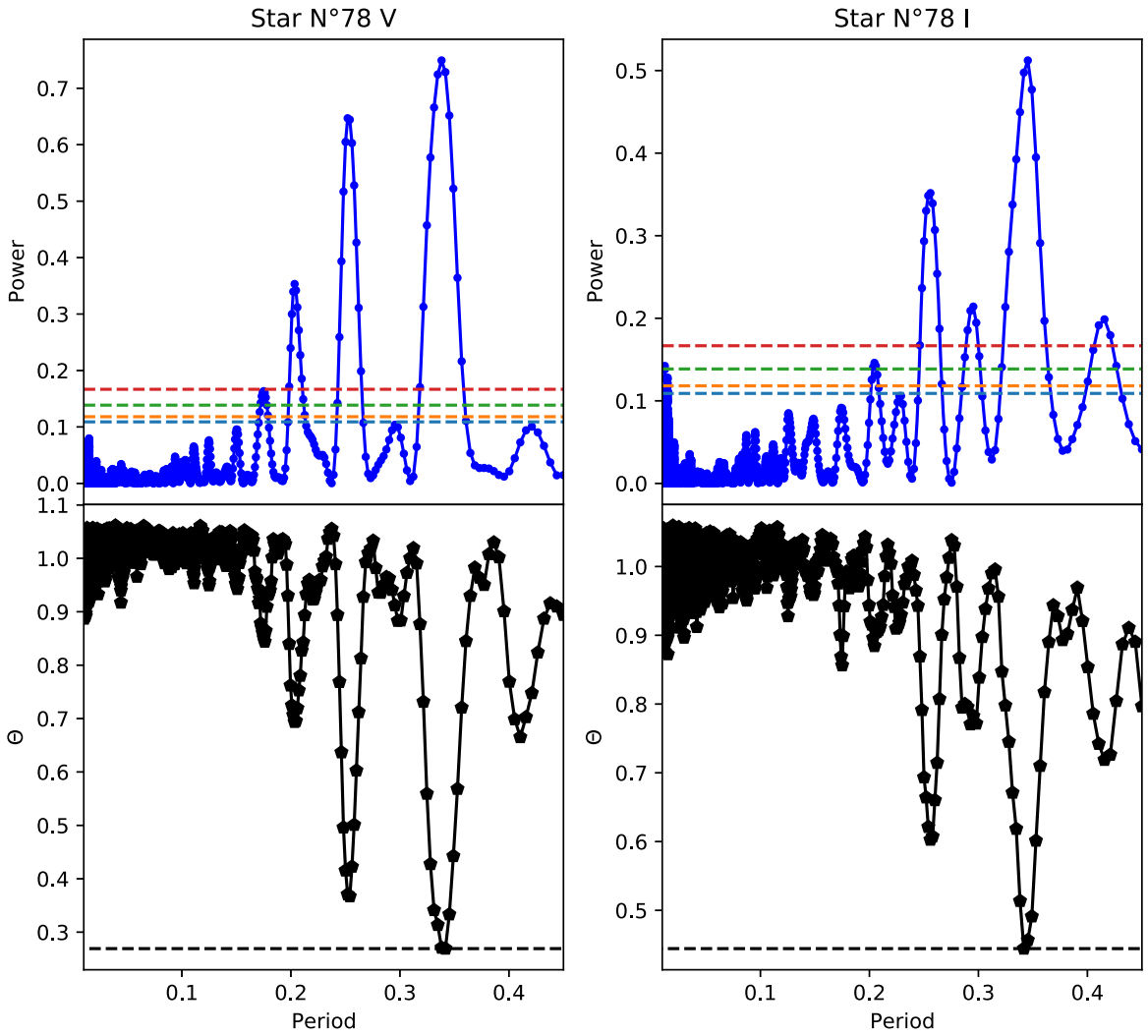


**Figure 1.** Resulting plots from the GLS (top panels) and PDM (bottom panels) analysis performed with the *PyAstronomy* package collection for *V* and *I* filters (left-hand and right-hand panels, respectively). Both results are from the initial period analysis of Star N°78. From the GLS analysis, one can see the different False-Alarm-Probability level thresholds indicated with the different colored dashed lines, with blue being 10%, orange 5%, green 1%, and red 0.1% probability. In the PDM analysis, the black-dashed line indicates the minimum value of Θ. Note that the GLS analysis for the *I* filter is the only one that marks a different period ($P = 0.0811$ day) compared to the ones marked by GLS in *V* filter and PDM for both filters.

**Table 2**
Significance *S* Values for *V* and *I* Filters for 88 Candidate Variable Stars and their Classification Based on the Criteria from Section 3.2

| ID star | R.A. (J2000.0) | Decl. (J2000.0) | $S_V$ | $S_I$ | Gaia DR3 Source id | Classification |
|---|---|---|---|---|---|---|
| 1 | 10:17:26.879 | −46:24:40.11 | +7.602 | +3.917 | 5413574936799801600 | Variable |
| 2 | 10:17:35.326 | −46:24:40.93 | −0.665 | +8.084 | | Possible |
| 3 | 10:17:27.430 | −46:24:46.50 | +7.787 | +3.011 | 5413574868080323328 | Variable |
| 4 | 10:17:37.482 | −46:24:41.01 | +4.205 | +6.849 | 5413575623996269696 | Variable |
| 5 | 10:17:31.383 | −46:24:50.00 | −0.480 | +2.667 | 5413576345549090304 | Dubious |
| 6 | 10:17:25.882 | −46:24:56.71 | +8.459 | +4.569 | 5413574936799786624 | Variable |
| 7 | 10:17:22.552 | −46:25:02.90 | +5.446 | +5.659 | 5413574898135625728 | Variable |
| | … | … | … | … | … | |

(This table is available in its entirety in machine-readable form.)

control of how many points we want to evaluate for the analysis with the resolution of the theta plot.

Before using these periodograms, we rejected three epochs taken on the fourth night for all of the stars observed in the *I* band. As in Albornoz et al. (2021), these epochs have been affected by bad photometry.

Figure 1 shows two periodograms in the *V* band (left-hand panel) and the *I* band (right-hand panel) for one star (N° 78) to illustrate the method. The upper panel shows the GLS periodogram, with the higher peak indicating the true period of the star. Furthermore, this periodogram carries out a False-Alarm-Probability (FAP), indicating the periods that are

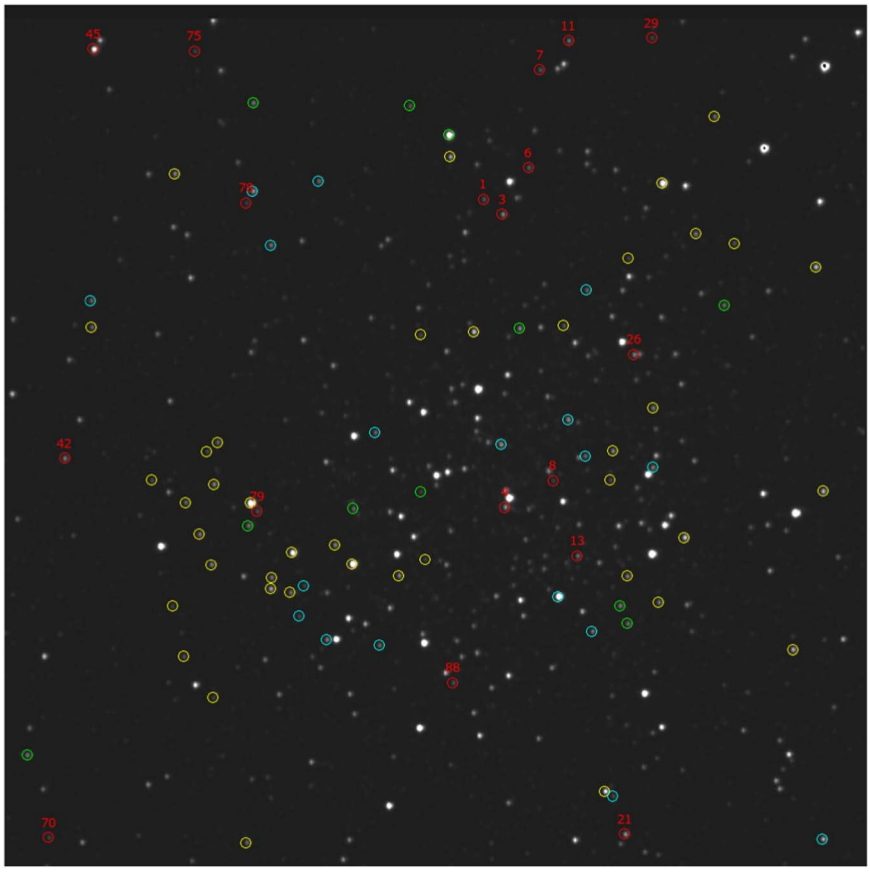


**Figure 2.** Finding chart of the area of NGC 3201 of the 88 giant stars studied. Red circles are the variable stars with the ID shown in Table 3. Cyan circles represent possible variable stars, green circles are dubious stars, and yellow circles indicate non-variable stars. West is up, north is to the left-hand, and the shown area is 5′.4 × 5′.4.

significant enough. Subsequently, the code also carried out the PDM periodogram (bottom panels), where we visualize the lowest peak to know the true period.

Although these periodograms indicate the existence of a periodic signal, we applied the following restrictions as done in Albornoz et al. (2021) to discard stars that are not variable from our sample:

1. From the parameters provided by the *PyAstronomy* package of the GLS analysis, the following inequality must be satisfied for $V$ and $I$ bands:

$$A \pm \sigma_A > \mathrm{rms}_{\mathrm{mag}},$$

   where $A$ is the amplitude, $\sigma_A$ its error and $\mathrm{rms}_{\mathrm{mag}}$ the root-mean square of the data.
2. The possible period indicated with the highest peak in the GLS periodogram for both filters must be above the FAP threshold of 0.1%.
3. The periods estimated with GLS and PDM periodogram must be similar for both bands.
4. The possible period must be present in both $V$ and $I$, and $P_V \approx P_I$.

Adopting these criteria, we selected 88 giant stars as candidate variable stars.

### 3.2. Statistical Analysis

In this section, we classify the 88 candidate variable stars as a variable, possible, dubious, and non-variable stars. For this, we performed the significance test from Albornoz et al. (2021). The procedure is as follows. We first calculate the mean magnitude difference for each star of the sample (the 255 targets) with the following equation:

$$\Delta M = M - \langle M \rangle,$$

where $\langle M \rangle$ is the mean magnitude of the star. We then calculate the variance for each filter and each one of the 167 non-variable stars discarded in the previous analysis

$$\sigma_M = \sqrt{\frac{\sum \Delta M^2}{N-1}},$$

and its error

$$\mathrm{err}_\sigma = \frac{\sigma_M}{\sqrt{2N}}.$$

We next calculate $\sigma_{\mathrm{M}}$ and $\mathrm{err}_\sigma$ for each one of the 88 candidate variables and each filter, and named them $\sigma_{\mathrm{Star}}$ and $\mathrm{err}_{\sigma_{\mathrm{Star}}}$. Finally, their significance $S$ is calculated as Equation (1)

$$S = \frac{\sigma_{\mathrm{Star}} - \sigma_{\mathrm{Non-Var}}}{\sqrt{\mathrm{err}^2_{\sigma_{\mathrm{Star}}} + \mathrm{err}^2_{\sigma_{\mathrm{Non-Var}}}}}. \quad (1)$$

Using the value of $S$ found in Equation (1), we proceed with the following criteria to classify our sample:

1. If $S < 2$ for both filters, then the star is cataloged as non-variable.

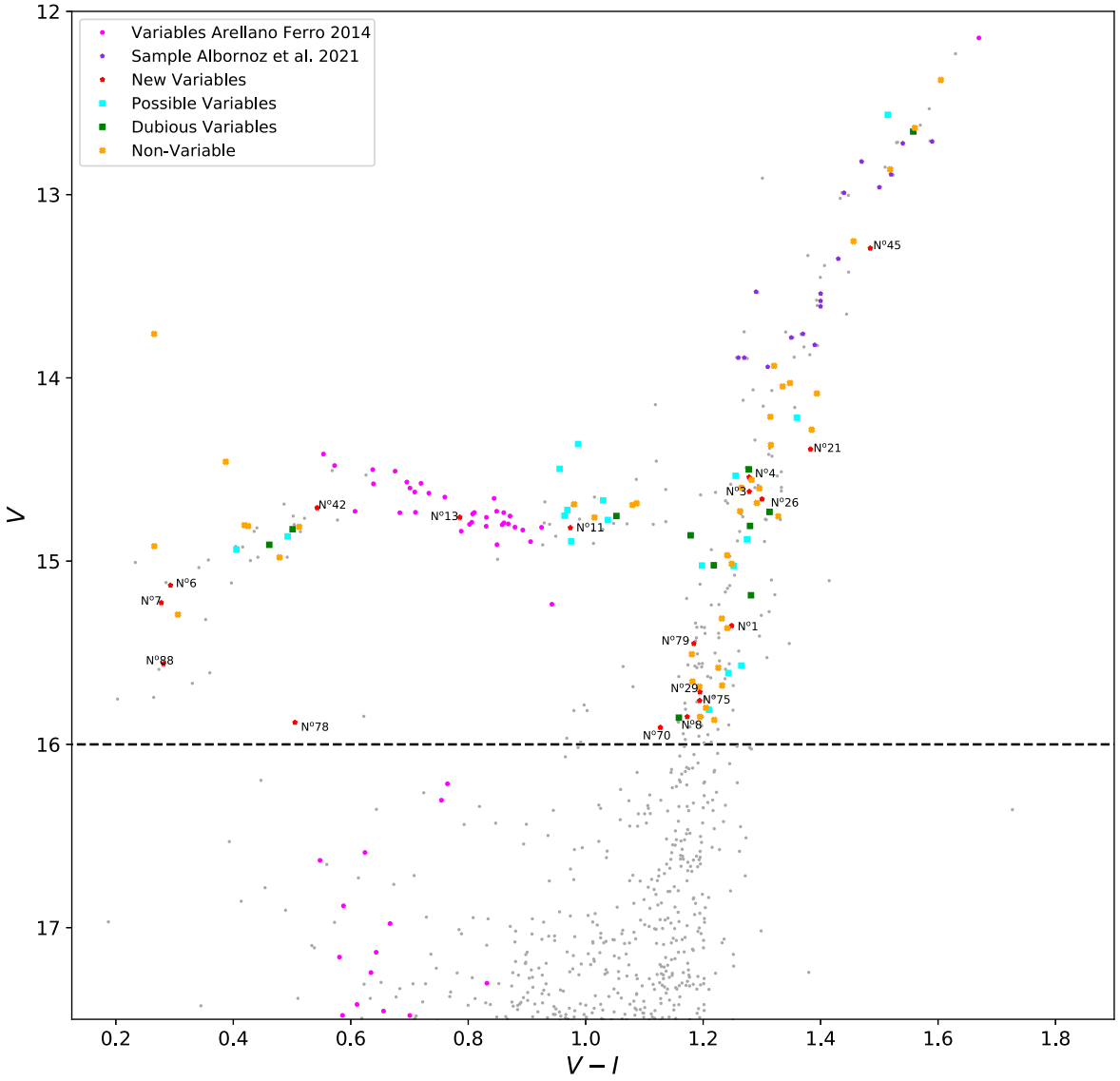


**Figure 3.** CMD of NGC 3201 displaying the 88 giant stars that were analyzed in this work with different markers based on their classification and with the same colors as in Figure 2. We also included the 17 giants from Albornoz et al. (2021) marked with brown dots and the confirmed variables from Arellano Ferro et al. (2014) marked with magenta dots. The ID corresponding to each variable star is indicated in their corresponding position of the CMD.

2. If $S > 3$ for both filters, then the star is cataloged as variable.
3. If $S > 3$ in only one of the filters, then the star is cataloged as possible variable.
4. If $2 < S < 3$ in one or both filters, then the star is cataloged as dubious variable and requires further analysis for confirmation.

From this test, we obtained our final classification for all candidates, where 18 stars were classified as variables, 18 as possible variables, 11 as dubious, and 41 stars were classified as non-variables. Table 2 shows the significance values for the 88 candidate variables along with their coordinates (R.A. and decl.) and classification according to the criteria previously presented. The 88 stars obtained from our final classification are shown in the Finding chart (Figure 2) and in the color–magnitude diagram (Figure 3), using the same colors (cyan circles represent possible variable stars, green circles are dubious stars, and yellow circles indicate non-variable stars).

In the final step, we needed to establish the membership of the cluster for these 88 stars. To do this, we obtained the proper motion data from the Gaia Mission Data Release 3 (Gaia Collaboration et al. 2016, 2023) and used the Tool for OPerations on Catalogues And Tables (TOPCAT, Taylor 2005) to match their positions (RA and DEC) with that of our own photometry. We were able to identify 84 out of the 88 targets. We then revised the astrometry to check if the shift in position was the same for all stars, and made an $I$ versus $R_p$ plot to check if our $I$ magnitude had a close match to the Gaia $R_p$ magnitude. From this analysis, we found three stars that have an $I$ magnitude that does not correspond to the Gaia $R_p$ magnitude (too bright or too faint) but we had no concrete reasons not to include them in this work because they are present in our photometry. Considering that the CMD does not present evident contamination from field stars, we kept all of our 88 stars for the following analysis and considered them all as cluster members. Figure 4 shows the complete proper motion map and a zoomed-in part where the cluster is located.

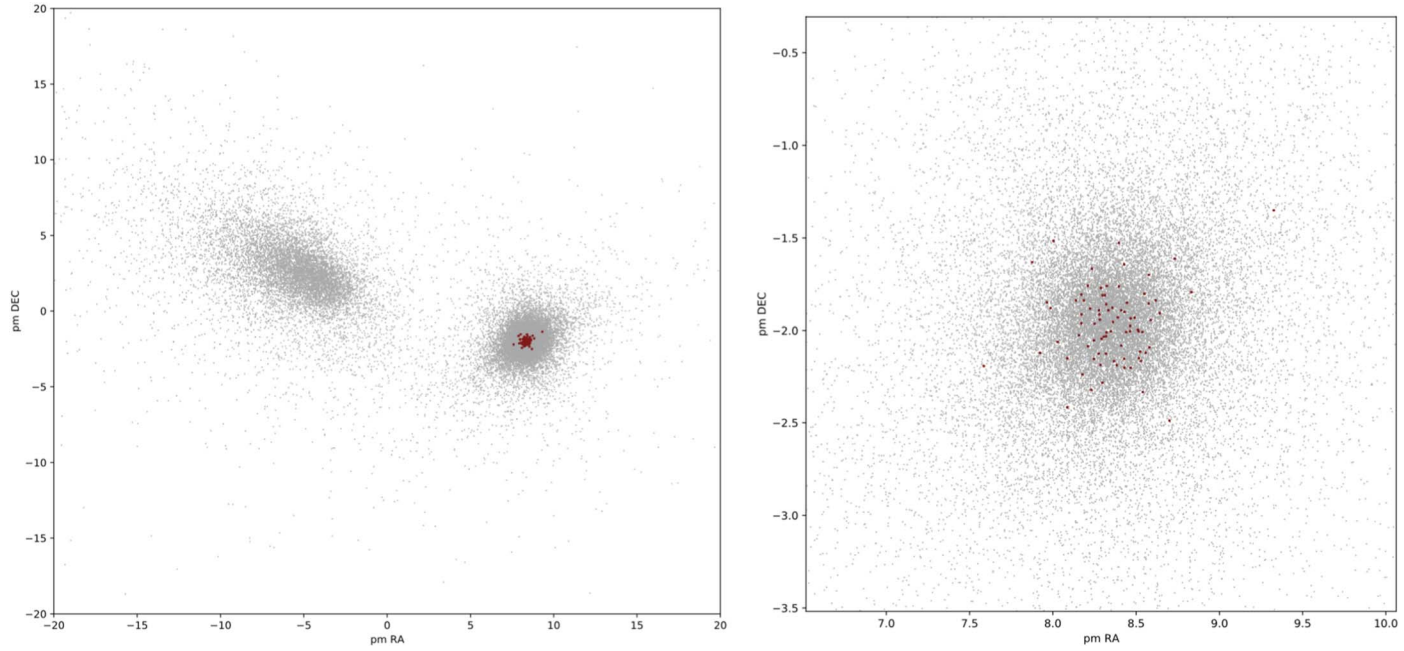


**Figure 4.** Plot displaying the proper motion of the stars from Gaia with the 84 stars that were determined as members of this cluster marked with maroon dots. Left-hand panel: complete proper motion map of all stars in a radius of 15′ from the center of NGC 3201. Right-hand panel: zoom of the proper motion map where the cluster is located with the 81 stars that were determined as members.

**Table 3**
Final Parameters for All Stars Classified as Variable from the Significance Test

| Star | $\langle M_V \rangle$ (mag) | $\langle M_I \rangle$ (mag) | $P_V$ (days) | $\sigma_{P_V}$ (days) | $A(V)$ (mag) | $\sigma_{A(V)}$ (mag) | $P_I$ (days) | $\sigma_{P_I}$ (days) | $A(I)$ (mag) | $\sigma_{A(I)}$ (mag) | Type |
|---|---|---|---|---|---|---|---|---|---|---|---|
| N° 1 | 15.35226 | 14.10365 | 0.24398 | 0.00189 | 0.01410 | 0.00165 | 0.24581 | 0.00235 | 0.00764 | 0.00105 | RGB |
| N° 3 | 14.62077 | 13.34217 | 0.32745 | 0.00200 | 0.01721 | 0.00146 | 0.31481 | 0.00242 | 0.00675 | 0.00067 | RGB |
| N° 4 | 14.54246 | 13.26423 | 0.34146 | 0.00328 | 0.01147 | 0.00126 | 0.34145 | 0.00371 | 0.01692 | 0.00217 | RGB |
| N° 6 | 15.13160 | 14.83851 | 0.32775 | 0.00249 | 0.01623 | 0.00173 | 0.34145 | 0.00325 | 0.01597 | 0.00164 | HB |
| N° 7 | 15.22733 | 14.94997 | 0.35636 | 0.00354 | 0.00992 | 0.00149 | 0.36028 | 0.00354 | 0.01531 | 0.00194 | HB |
| N° 8 | 15.84971 | 14.67691 | 0.34146 | 0.00235 | 0.01390 | 0.00106 | 0.34506 | 0.00405 | 0.00636 | 0.00095 | RGB |
| N° 11 | 14.81805 | 13.84414 | 0.54748 | 0.00365 | 0.02575 | 0.00128 | 0.53842 | 0.00330 | 0.03179 | 0.00150 | HB |
| N° 13 | 14.76093 | 13.97512 | 0.36028 | 0.00116 | 0.70348 | 0.02895 | 0.35629 | 0.00112 | 0.44557 | 0.01933 | HB |
| N° 21 | 14.38889 | 13.00606 | 0.35766 | 0.00454 | 0.01763 | 0.00182 | 0.35763 | 0.00297 | 0.02608 | 0.00219 | RGB |
| N° 26 | 14.66172 | 13.36148 | 0.58681 | 0.00400 | 0.06422 | 0.00306 | 0.58675 | 0.00401 | 0.03415 | 0.00169 | RGB |
| N° 29 | 15.71488 | 14.52026 | 0.24957 | 0.00138 | 0.01518 | 0.00140 | 0.24956 | 0.00150 | 0.01734 | 0.00167 | RGB |
| N° 42 | 14.70897 | 14.16622 | 0.37403 | 0.00198 | 0.02182 | 0.00138 | 0.37388 | 0.00432 | 0.01656 | 0.00138 | Blue HB |
| N° 45 | 13.29256 | 11.80799 | 0.14259 | 0.00056 | 0.01404 | 0.00146 | 0.14262 | 0.00071 | 0.02604 | 0.00368 | RGB |
| N° 70 | 15.90760 | 14.78043 | 0.34346 | 0.00193 | 0.03170 | 0.00210 | 0.34918 | 0.00345 | 0.01648 | 0.00138 | sub-giant(?) |
| N° 75 | 15.76161 | 14.56750 | 0.32977 | 0.00232 | 0.02146 | 0.00198 | 0.32854 | 0.00128 | 0.03480 | 0.00194 | low-RGB |
| N° 78 | 15.88062 | 15.37553 | 0.33688 | 0.00139 | 0.02648 | 0.00122 | 0.34489 | 0.00192 | 0.02092 | 0.00158 | Blue HB(?) |
| N° 79 | 15.45002 | 14.26593 | 0.34146 | 0.00421 | 0.01168 | 0.00146 | 0.34145 | 0.00759 | 0.01736 | 0.00298 | low-RGB |
| N° 88 | 15.56012 | 15.27911 | 0.55831 | 0.00529 | 0.04034 | 0.00326 | 0.55992 | 0.00562 | 0.03414 | 0.00280 | Blue HB |

**Note.** Column 12 shows the location of the star in the CMD presented in Figure 3.

(This table is available in machine-readable form.)

The 84 stars for which we could find a match with the Gaia database are marked with maroon dots.

## 4. Analysis of the Sample

In this section, we present the analysis of all stars that were classified as either variable, possible variable, or dubious variable, which were all determined as cluster members. For the two latter cases (possible and dubious variables), we re-performed the previous period analysis while also employing the PDM tool from the IRAF (Tody 1986) package. This is intended to re-evaluate the periods considered in our initial analysis from Section 3 and confirm—in the case of stars classified as a possible and dubious variable—if they can be considered for future photometric observations, or discard them if they show inconsistencies in IRAF PDM and our previous analysis (such cases are described in Section 4.5). The final parameters for all three classifications are presented in Tables 3 (variables) and 4 (possible and dubious), with $\langle M_I \rangle$ and $\langle M_V \rangle$ being the mean magnitudes in filters $I$ and $V$, respectively, while $P_V$ and $P_I$ are the periods in both filters, and $A$

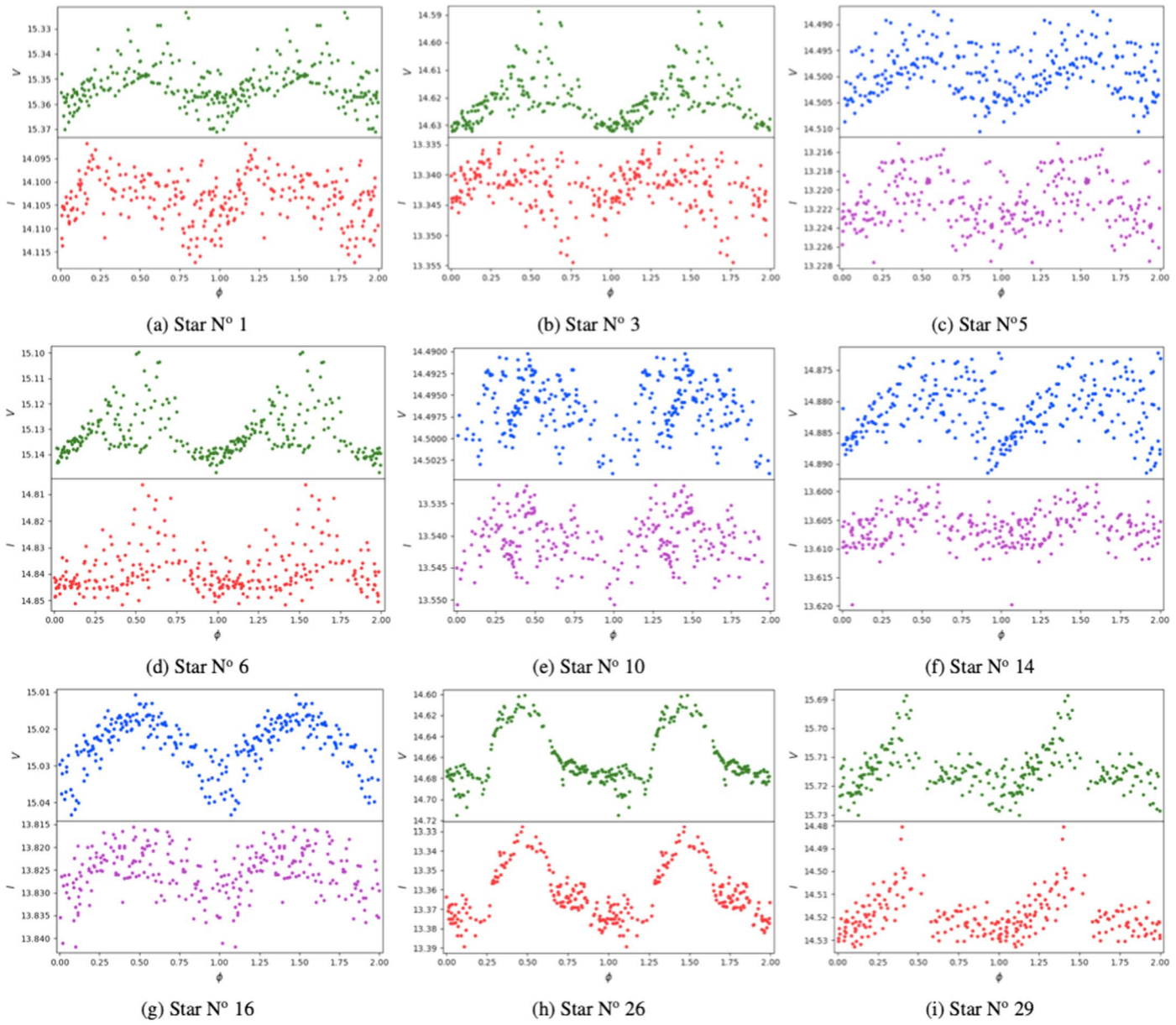


**Figure 5.** Phased LCs of the first nine out of our 13 stars corresponding to Group 1. The top panel of each phased LC corresponds to the phased curve in the *V* filter and the bottom panel is the phased curve in the *I* filter. The plots with colors green and red correspond to stars classified as variable, while the plots with colors blue and magenta are for stars classified as possible or dubious variables.

($V$) and $A(I)$ the amplitudes in each filter—each of them with their respective errors—found through the GLS method described in Section 3.1. From our final analysis performed for these stars, we grouped them into four groups based on the shape and pattern of their phased LCs. The characteristics of each group are described in the following subsections. The individual phased LCs for each star are displayed in Figures 5 and 6 for Group 1, Figure 7 for Group 2, Figure 8 for Group 3, and Figure 9 for Group 4. Each plot has a top and bottom panel showing the phased LC in $V$ and $I$ filter, respectively, and the colors correspond to variables (green and red) or to possible or dubious variables (blue and magenta).

### 4.1. Group 1

This group is composed of 13 stars, which are characterized by an even rise and fall in their LCs. We normalized phased LCs to group these stars according to the shape of their light curve, as shown Figure 10(a). Of the stars classified as variable, N° 1, 3, 29, and 75, are located in the RGB, while stars N° 6, 42, and 78 are located in the HB, as shown in Figure 3. Stars N° 42 and 78 have a phased LC (Figure 6(b) and (d)) that presents a shape typical of a RR Lyrae, and their phased LC is also similar (in the $I$ filter) to that of Star N° 17 from Albornoz et al. (2021) and they have a comparable period ($P = 0.3535 \pm 0.0035$ day for Star N° 17). According to the Bailey diagram by Arellano Ferro et al. (2014), Star N° 42 could be a RR Lyrae c-type. Although the amplitude is small to be classified as this type of variable star, Wallace et al. (2019) found RR Lyrae of ultralow amplitude with similar characteristics to those of Star N° 42 and which were also located in the HB region of the globular cluster.

In addition, we can note in Figure 6(b) in the $V$ filter that this star has a double maximum, which is a characteristic phenomenon of the Blazko effect (Blažko 1907). However, it

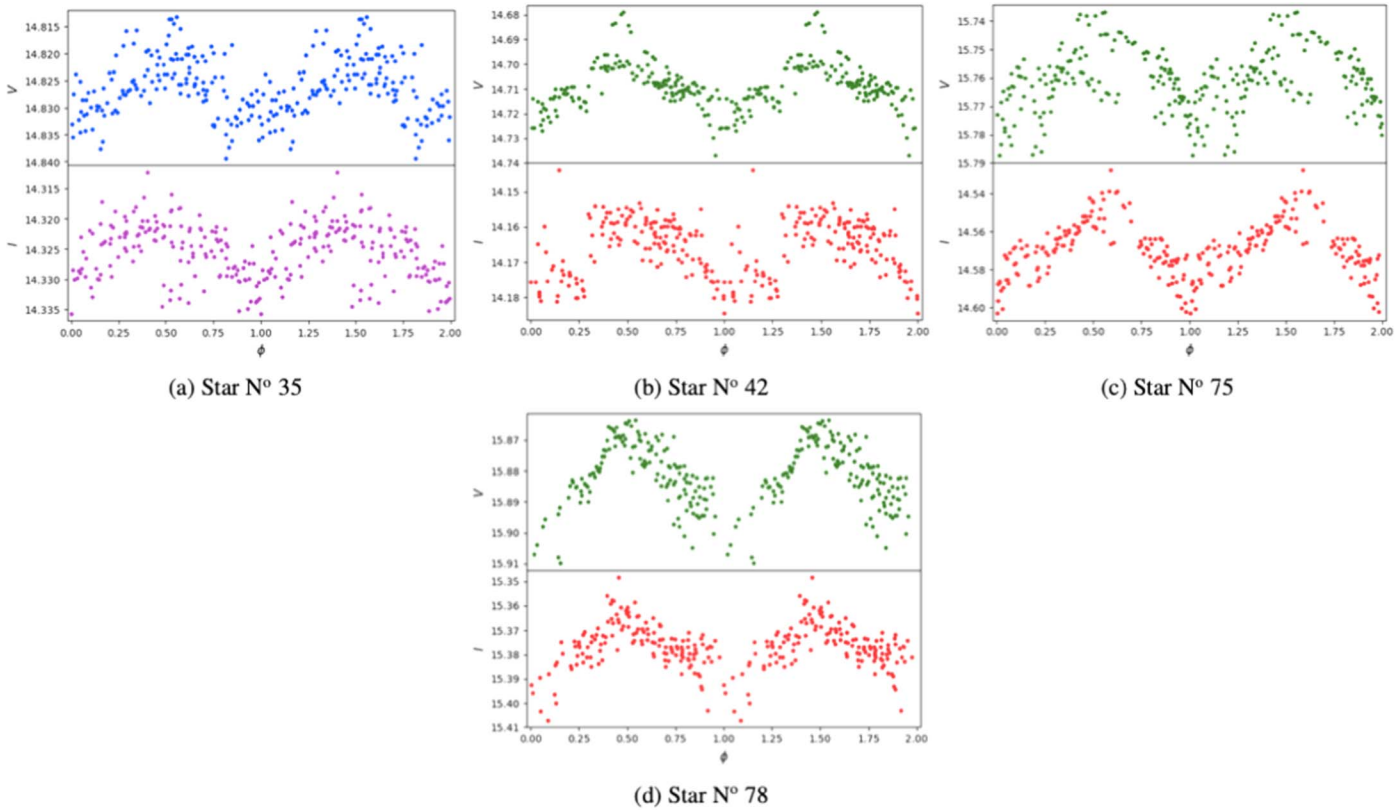


**Figure 6.** Phased LCs of the last four out of our 13 variable stars shown in Table 3. Top and bottom panels for each plot, as well as the colors, are the same as in Figure 5.

**Table 4**
Final Parameters for All Stars Classified as Possible Variable and Dubious from the Significance Test

| Star | $\langle M_V \rangle$ (mag) | $\langle M_I \rangle$ (mag) | $P_V$ (days) | $\sigma_{P_V}$ (days) | $A(V)$ (mag) | $\sigma_{A(V)}$ (mag) | $P_I$ (days) | $\sigma_{P_I}$ (days) | $A(I)$ (mag) | $\sigma_{A(I)}$ (mag) | Type |
|---|---|---|---|---|---|---|---|---|---|---|---|
| N° 2 | 14.53438 | 13.27906 | 0.347627 | 0.00314 | 0.00894 | 0.00075 | 0.343950 | 0.00445 | 0.00400 | 0.00066 | RGB |
| N° 5 | 14.49898 | 13.22128 | 0.141820 | 0.00079 | 0.00660 | 0.00095 | 0.142429 | 0.00091 | 0.00368 | 0.00056 | RGB |
| N° 9 | 12.56435 | 11.04999 | 0.748077 | 0.01173 | 0.01140 | 0.00092 | 0.731281 | 0.00868 | 0.00920 | 0.00070 | AGB |
| N° 10 | 14.49629 | 13.54067 | 0.566465 | 0.01893 | 0.00456 | 0.00068 | 0.521234 | 0.01214 | 0.00749 | 0.00082 | HB |
| N° 14 | 14.88109 | 13.60649 | 0.251494 | 0.00254 | 0.00630 | 0.00091 | 0.245805 | 0.00195 | 0.00481 | 0.00060 | RGB |
| N° 15 | 14.75235 | 13.78835 | 0.345067 | 0.00257 | 0.00772 | 0.00070 | 0.348740 | 0.00324 | 0.00576 | 0.00069 | HB |
| N° 16 | 15.02391 | 13.82575 | 0.148554 | 0.00028 | 0.01681 | 0.00093 | 0.149215 | 0.00060 | 0.00868 | 0.00103 | RGB |
| N° 20 | 14.75364 | 13.70129 | 0.334467 | 0.00180 | 0.01161 | 0.00075 | 0.337914 | 0.00284 | 0.00916 | 0.00071 | HB |
| N° 23 | 14.91074 | 14.44947 | 0.337927 | 0.00228 | 0.01125 | 0.00086 | 0.341447 | 0.00309 | 0.01285 | 0.00123 | HB |
| N° 24 | 15.57001 | 14.30497 | 0.255427 | 0.00182 | 0.00974 | 0.00127 | 0.267995 | 0.00209 | 0.01317 | 0.00142 | RGB |
| N° 27 | 14.66851 | 13.63878 | 0.538442 | 0.00492 | 0.02511 | 0.00169 | 0.538382 | 0.01447 | 0.00749 | 0.00109 | HB |
| N° 35 | 14.82586 | 14.32489 | 0.261563 | 0.00156 | 0.01028 | 0.00097 | 0.263667 | 0.00226 | 0.00713 | 0.00091 | HB |
| N° 39 | 14.21723 | 12.85764 | 0.142852 | 0.00047 | 0.00901 | 0.00089 | 0.142838 | 0.00037 | 0.01650 | 0.00123 | RGB |
| N° 41 | 14.85912 | 13.68030 | 0.34421 | 0.00247 | 0.01280 | 0.00088 | 0.35301 | 0.00455 | 0.00386 | 0.00066 | RGB |
| N° 43 | 14.86504 | 14.37253 | 0.49914 | 0.00494 | 0.01364 | 0.00090 | 0.42177 | 0.00601 | 0.00910 | 0.00128 | Blue HB |
| N° 52 | 14.80792 | 13.52807 | 0.34902 | 0.00285 | 0.00960 | 0.00104 | 0.34532 | 0.00308 | 0.01056 | 0.00116 | RGB |
| N° 54 | 14.36097 | 13.37391 | 0.33688 | 0.00153 | 0.01820 | 0.00096 | 0.34421 | 0.00192 | 0.00918 | 0.00066 | Red HB |
| N° 55 | 14.73165 | 13.41847 | 0.20719 | 0.00178 | 0.00816 | 0.00112 | 0.20331 | 0.00121 | 0.01020 | 0.00126 | RGB |
| N° 57 | 14.77531 | 13.73759 | 0.33108 | 0.00226 | 0.01344 | 0.00112 | 0.33445 | 0.00329 | 0.00950 | 0.00096 | RGB |
| N° 61 | 14.89206 | 13.91662 | 0.24663 | 0.00103 | 0.01722 | 0.00114 | 0.24502 | 0.00202 | 0.00490 | 0.00076 | Red HB |
| N° 62 | 14.72121 | 13.75242 | 0.52470 | 0.00668 | 0.00880 | 0.00094 | 0.53325 | 0.00726 | 0.01380 | 0.00164 | Red HB |
| N° 65 | 14.93640 | 14.53118 | 0.33216 | 0.00308 | 0.01312 | 0.00118 | 0.34195 | 0.00656 | 0.00722 | 0.00120 | Blue HB |
| N° 67 | 12.65576 | 11.09805 | 0.53844 | 0.00363 | 0.01658 | 0.00100 | 0.52965 | 0.00439 | 0.01330 | 0.00082 | RGB |
| N° 80 | 15.61064 | 14.36764 | 0.16262 | 0.00071 | 0.01820 | 0.00116 | 0.11882 | 0.00048 | 0.00808 | 0.00140 | low-RGB |
| N° 81 | 15.81118 | 14.60119 | 0.16064 | 0.00109 | 0.00812 | 0.00144 | 0.19402 | 0.00168 | 0.00874 | 0.00160 | low-RGB |
| N° 82 | 15.02232 | 13.80414 | 0.33688 | 0.00304 | 0.01170 | 0.00096 | 0.33701 | 0.00251 | 0.00612 | 0.00062 | RGB |
| N° 83 | 15.02648 | 13.77445 | 0.16998 | 0.00112 | 0.00796 | 0.00126 | 0.16882 | 0.00081 | 0.01314 | 0.00150 | RGB |
| N° 84 | 15.18617 | 13.90468 | 0.34902 | 0.00305 | 0.00848 | 0.00104 | 0.34170 | 0.00334 | 0.01332 | 0.00144 | RGB |
| N° 86 | 15.85423 | 14.69551 | 0.34569 | 0.00335 | 0.00906 | 0.00098 | 0.34175 | 0.00504 | 0.00968 | 0.00156 | sub-giant(?) |

(This table is available in machine-readable form.)

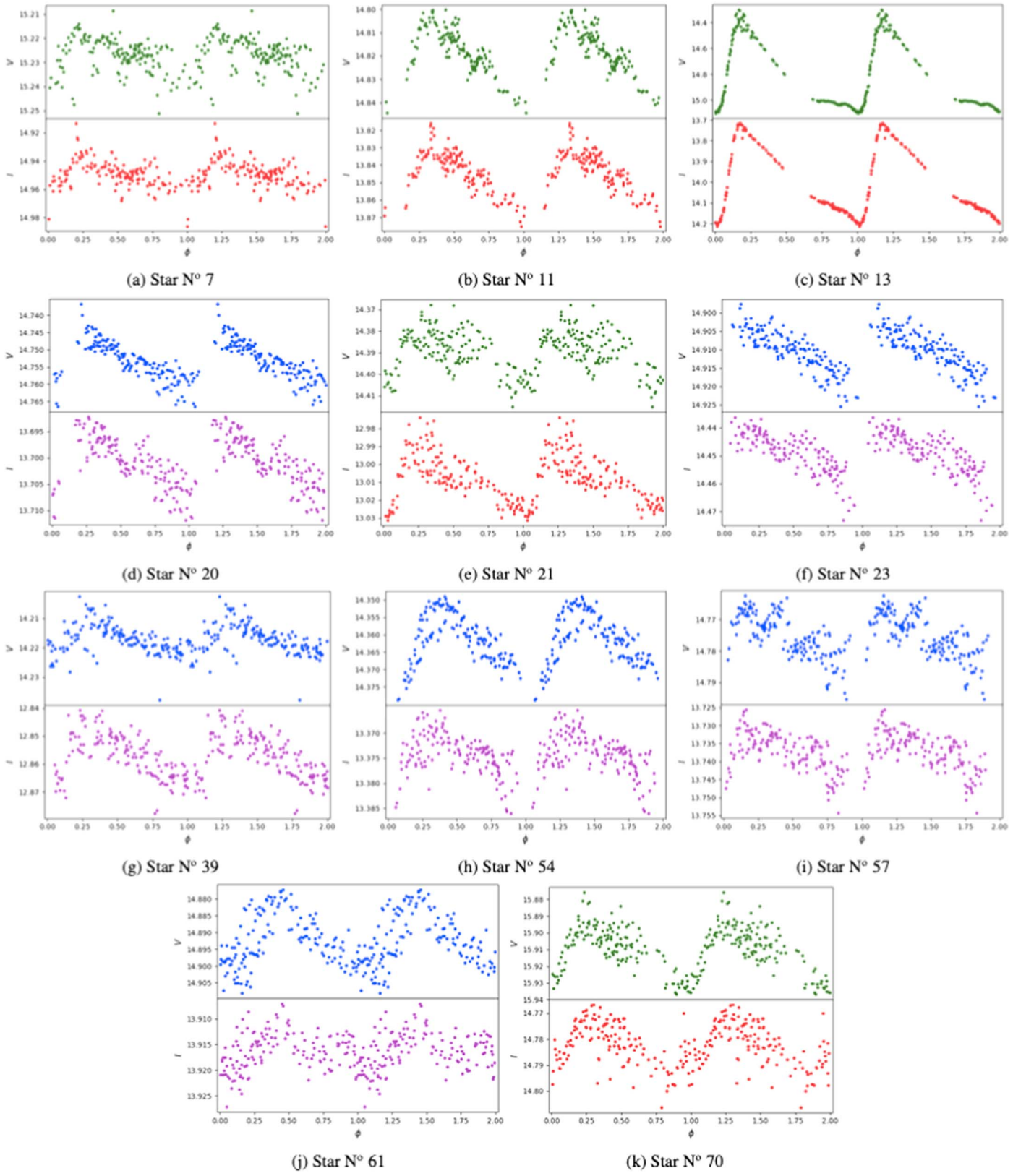


**Figure 7.** Phased LC of 10 stars that are considered for Group 2. The top and bottom panels of each individual plot and its corresponding colors are the same as in the case of Figure 5.

is difficult to provide a clear classification for Star N°78 because its amplitude $A(V)$ and $A(I)$ are quite small compared to those of typical RR Lyrae.

Among the stars labeled as possible variables, N° 10 is located in the HB of the cluster, while stars N° 14 and 16 are in the RGB. Finally, stars N° 5 and 35, classified as dubious

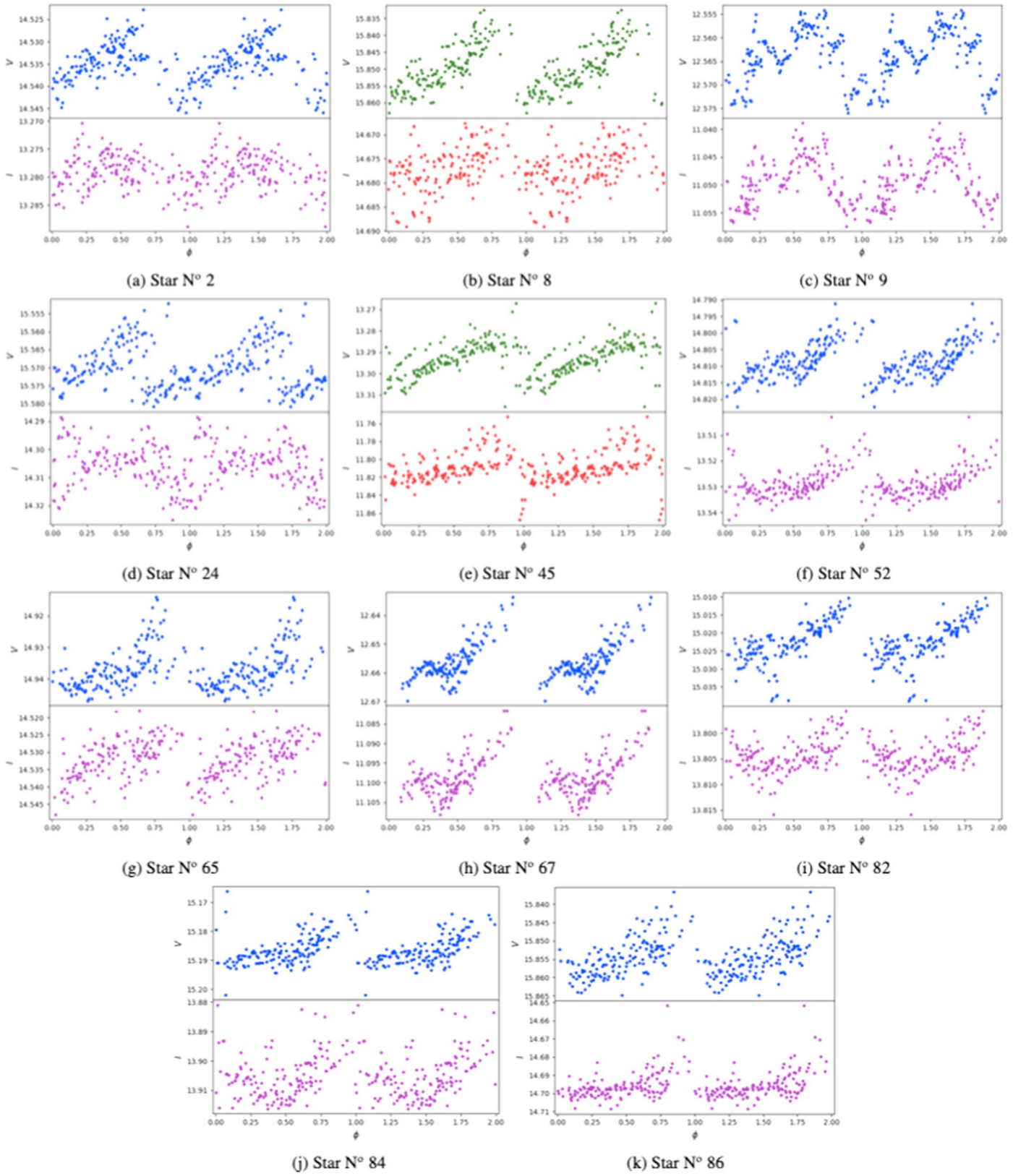


**Figure 8.** Phased LC of the 11 stars from Group 3. The colors shown in the top and bottom panels of each plot are the same as those presented in Figure 5.

variables, are located in the RGB and HB regions of the CMD, respectively.

Since these stars have a short period and low amplitude, we cannot classify them among the known variable stars. We also note that their LCs do not match the shape of those of known variable stars. They may be pulsating stars, but the classification is uncertain.

A curious case of this group is the new variable Star N° 26, whose phased LC (Figure 5(h)) shows a notorious variable behavior with a peculiar shape, and displays the highest period

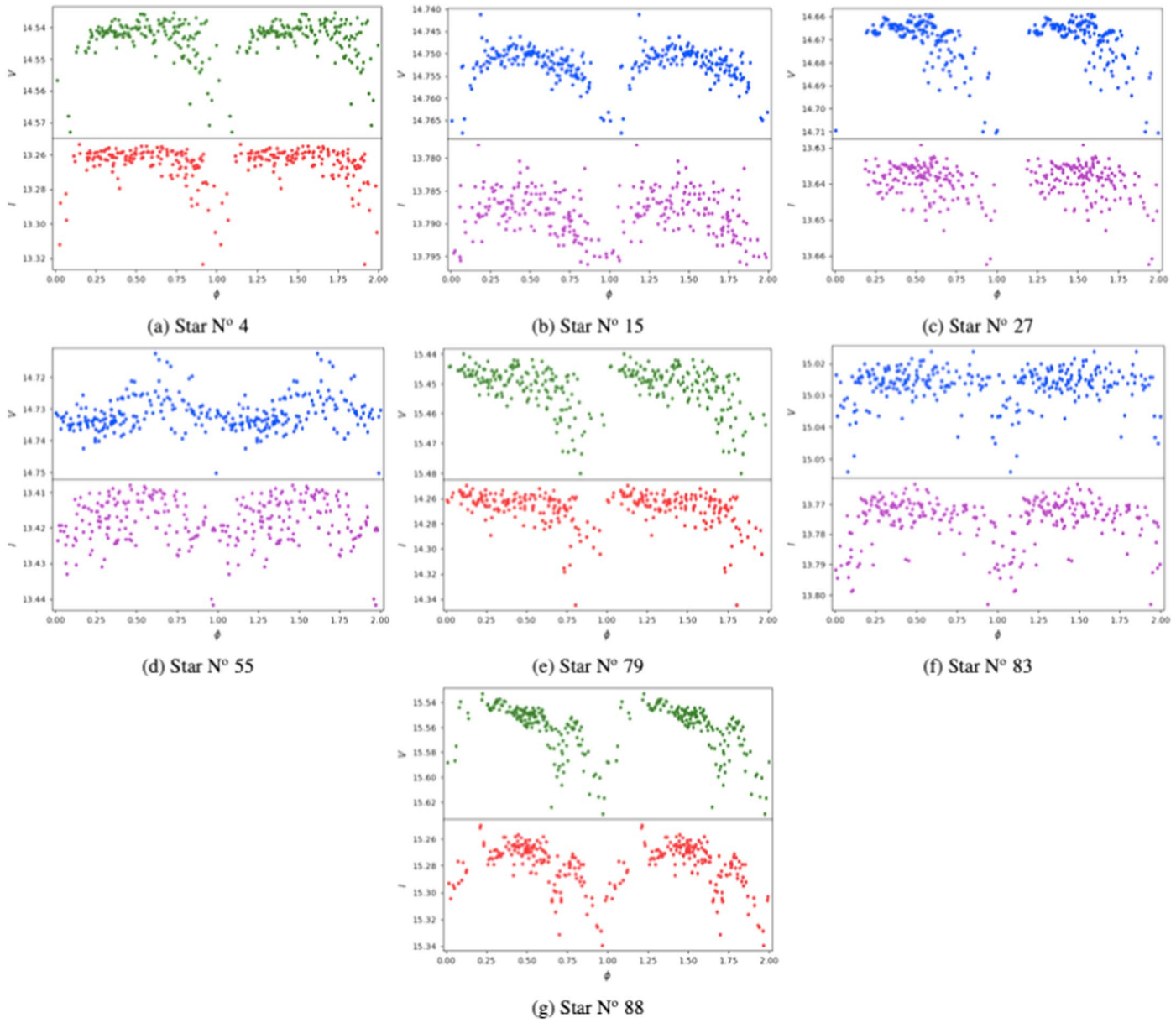


**Figure 9.** Phased LC of the seven stars that correspond to Group 4. Like the previous groups, the colors shown in the top and bottom panels of each plot are the same as those presented in Figure 5, based on the classification of each star.

($P_V = 0.5868$ and $P_I = 0.5867$) in our sample and the second highest amplitude in $V$ ($A(V) = 0.06422$), with Star N° 13 being the one with the highest amplitude. In addition, Table 3 shows that this star is located in the middle of the RGB, at the level of the HB. Even though its phased LC shape is clear, we cannot make a clear classification due to its low amplitude, like some of our other variables.

### 4.2. Group 2

This second group consists of 11 stars that share a similar pattern in their phased LCs, and like in the case of Section 4.1 has stars classified as variable (N° 7, 11, 13, 21, and 70), possible variable (N° 39, 54, 57, and 61), and dubious variable (N° 20 and 23). These stars are located in different sections of the CMD from Figure 3, with three stars in the RGB (N° 21, 39, and 57), seven stars in the HB (N° 7, 11, 13, 20, 23, 54, and 61), and one in the sub-giant branch (N° 70).

The shape of their phased LC is characterized mostly by a fast rise in magnitude with a slower fall, which is similar to the LCs from known variables such as RR Lyrae ab stars and Cepheids. One thing to note is that they have low amplitudes like the new type of variable star reported by Albornoz et al. (2021).

The most peculiar star from this group is Star N° 13, which is shown in Figure 7(c), being similar to Star N° 1 of Albornoz et al. (2021). Because of its period ($P_V = 0.36028$ and $P_I = 0.35629$), amplitude ($A(V) = 0.70348$ and $A(I) = 0.44557$), and the shape of the phased LC, we suggest it to be a RR Lyrae ab-type star with a Blazhko effect (Blažko 1907). This star is located in the region of the HB, in the middle of the sample of RR Lyrae variable stars reported by Arellano Ferro et al. (2014). This star does not present previous studies on its variability, which might have been due to its low amplitude.

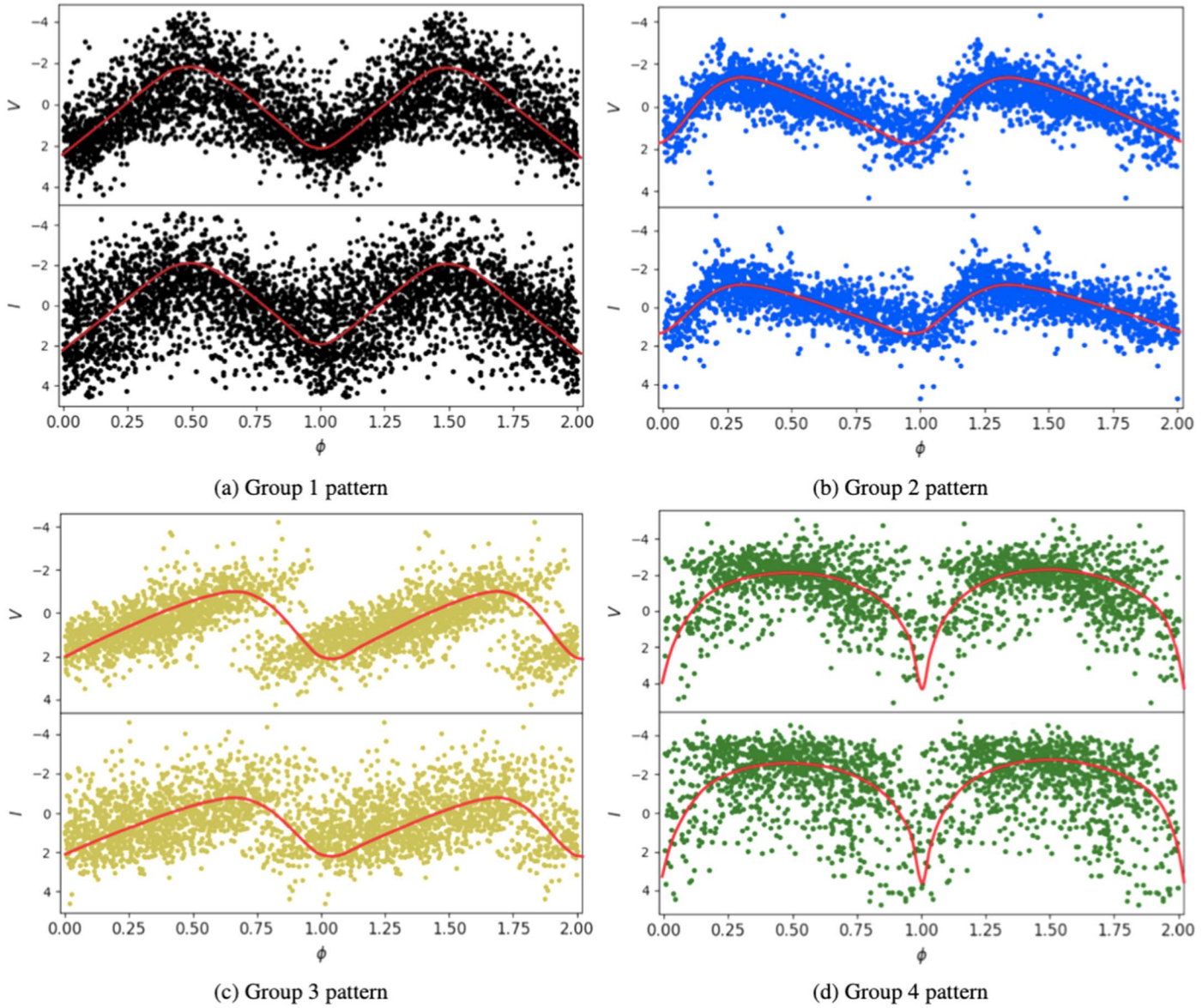


**Figure 10.** Top: normalized phased LCs in $V$ for all stars that were labeled in Group 1 (left-hand panel) and Group 2 (right-hand panel). Bottom: normalized phased LCs in $V$ for stars labeled in Group 3 (left-hand panel) and Group 4 (right-hand panel). The red line in all plots shows the best fit of the pattern of each group of stars.

Likewise, we suggest that according to its period ($P_V = 0.54748$ and $P_I = 0.53842$), position in the CMD (HB region, see Figure 3) and the shape of the phased LC (Figure 7(b)), the Star N° 11 it to be a RR Lyrae ab-type star. Although its amplitude is small ($A(V) = 0.02575$ and $A(I) = 0.03179$), as previously mentioned, there are already reports of RR Lyrae with ultralow amplitude (Wallace et al. 2019) also positioned in the HB region.

### 4.3. Group 3

This third group of stars also has 11 stars (N° 2, 8, 9, 24, 45, 52, 65, 67, 82, 84, and 86). The characteristic that defines this group's phased LCs is their slow rise in magnitude with a steep fall at the end, like a mirror image of Group 2, with each individual phased LC being shown in Figure 8.

Of the stars of this group, two are classified as variable (N° 8 and 45), four as possible (N° 2, 9, 24, and 65), and five as dubious (N° 52, 67, 82, 84, and 86). Eight stars are located in the RGB (N° 2, 8, 24, 45, 52, 67, 82, and 84), one in the AGB region (N° 9), one in the HB (N° 65), and one located in the lowest part of the giant branch (Star N° 86). Most of these stars have low amplitudes, which makes them hard to classify even though their periods are similar to known variable stars with similar light-curve shape, such as RR Lyrae.

One of the most interesting cases of this group is the possible variable Star N° 9, which has a phased LC (Figure 7(c)) that shows maximum magnitude asymmetry. This bump in the LC is probably caused by interference between two radial pulsation modes, known as Hertzsprung progression or a spot. Therefore, the period ($P_V = 0.748077$) and amplitude ($A(V) = 0.01140$) are typical of the new type of variable star reported by Albornoz et al. (2021).

### 4.4. Group 4

This last group consist of seven stars: three variables (N° 4, 79, and 88), three possible variables (N° 15, 27, and 83), and

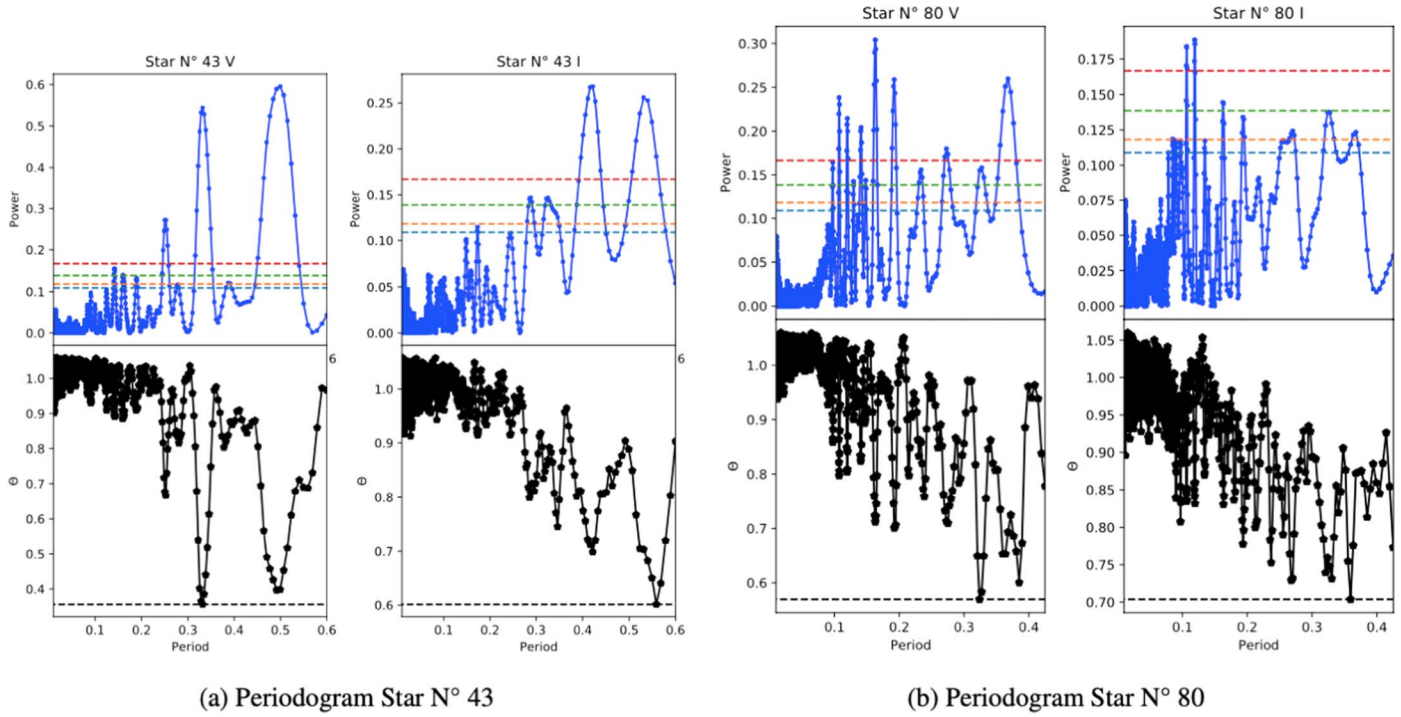


**Figure 11.** Left-hand panel: periodogram of Star N° 43 showing the period discrepancy between filters and methods. Right-hand panel: periodogram of Star N° 80 showing the discrepancy between filters and period analysis methods, particularly in *I*.

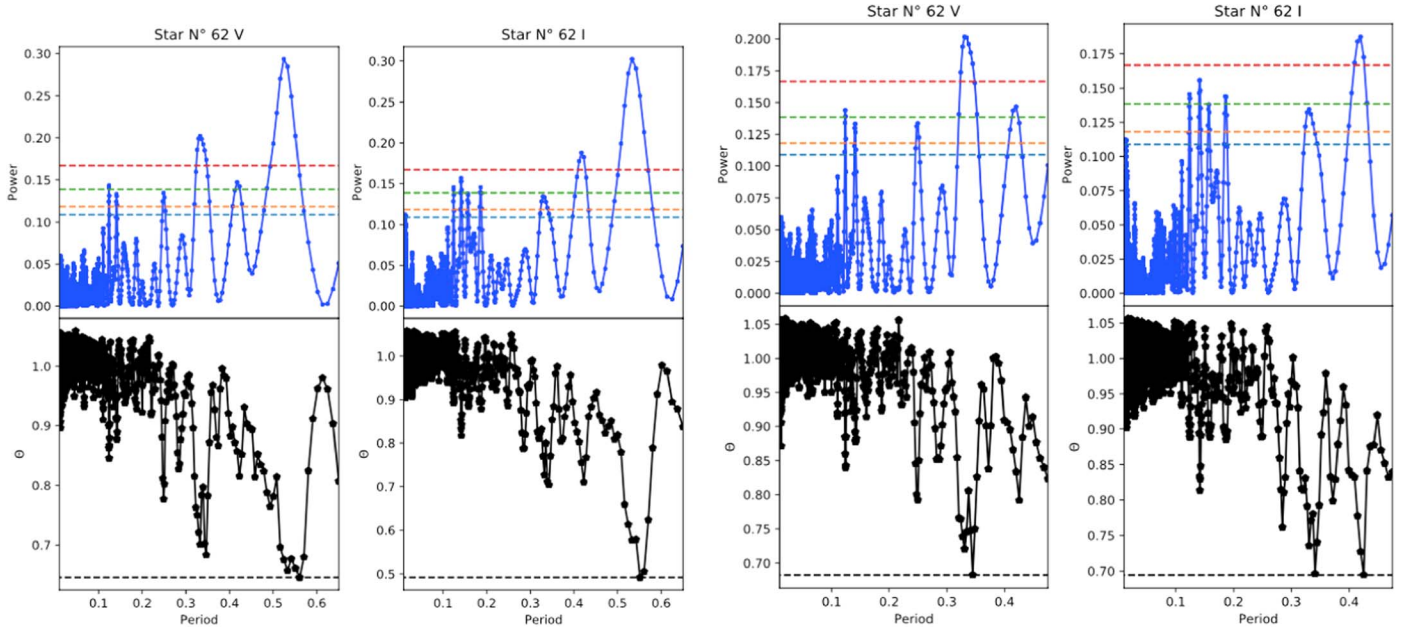


**Figure 12.** Left-hand panel: periodogram of Star N° 62 showing the period initially labeled as possible, and how in *V* the PDM have a broad and dual peak. Right-hand panel: periodogram of Star N° 62 after discarding the initial possible period due to the IRAF PDM analysis, showing a clear difference in periods.

one dubious variable (N° 55). In this group, similar to the three previous cases, we have stars located both in the RGB (N° 4, 79, 55, and 83) and the HB (N° 15, 27, and 88) of the CMD from Figure 3. As we see from Figure 9, the phased light curve of these stars is curved, which means that we can classify them among the known existing kind of variables, as a contact binaries, i.e., W Ursar Majoris.

Finally, a peculiar case of this group is the dubious variable Star N° 55 that is located in the RGB, whose periodogram showed that the possible period was $P \sim 0.25$ days but in the IRAF PDM analysis the period had a peak of $P \sim 0.26$ in the *I* filter. However the same analysis showed a bump instead of a complete peak, and the second peak had $P = 0.20719$ days. The values presented in Table 4 are the ones that we obtained with the IRAF PDM analysis.

### 4.5. Discarded Candidates

In this section, we present stars classified as either possible or dubious variable but which we discarded from being

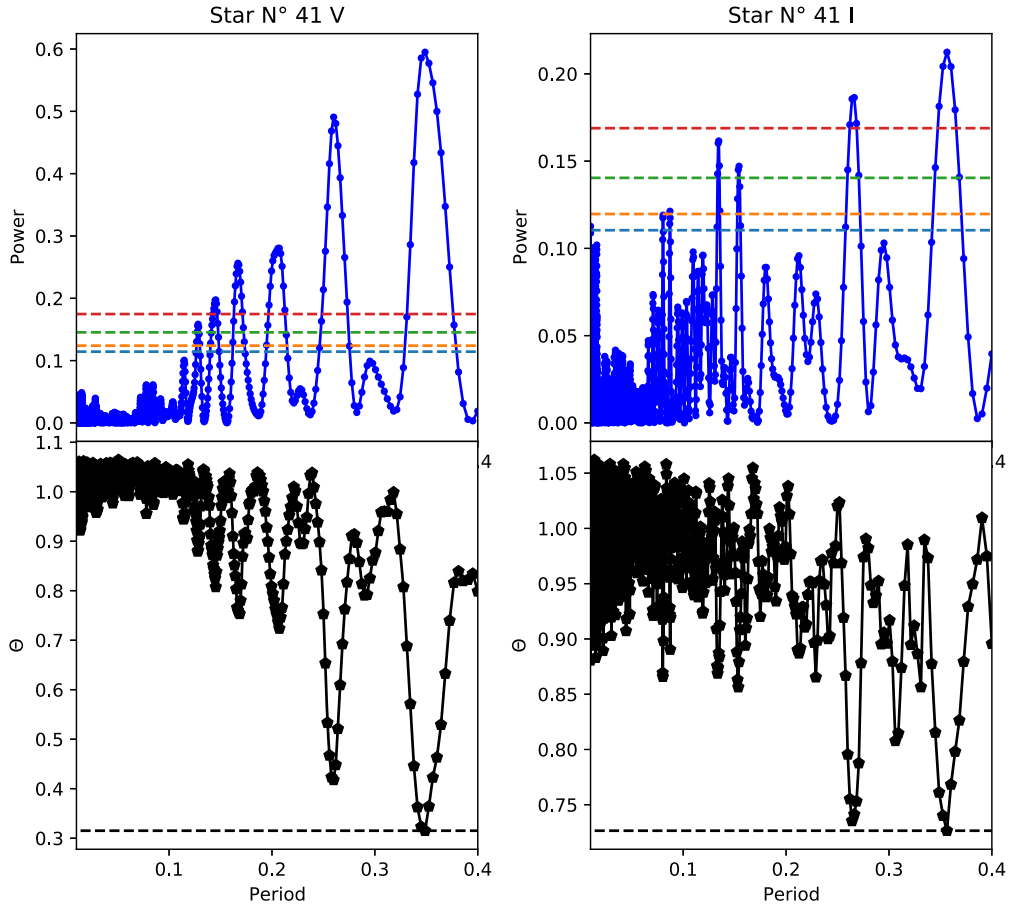


**Figure 13.** Periodogram obtained from the GLS and PDM analysis for Star N°41.

variable because of their inconsistencies when preforming our PDM analysis with IRAF and our previous analysis detailed in Section 3.

Stars N° 43, 62, 80, and 81 were at first considered as candidate variables from our initial analysis and labeled as possible variable in our significance test. However, they were discarded from being possible variables with our later analysis based on the PDM analysis in IRAF. Note that the first two are located in the HB of the CMD, while the latter two are in the lowest section of the RGB. Star N° 43 showed different $I$ and $V$ filter periods ($P_V = 0.49914$ days versus $P_I = 0.42177$ days). Furthermore, the best periods for our revised GLS analysis showed a difference in periods, as seen in Table 4, with Figure 11 (left-hand panel) showing the periodogram of this star.

The next case is Star N° 62, which at first the GLS and PDM analysis showed that the possible period was at $P \sim 0.54$ with good agreement between filters (see Table 4). However, the IRAF PDM showed that in $V$ it had a notorious broad peak, which led us to discard this period. Furthermore, when re-performing our analysis with this period discarded, we noticed that the other possible periods for this star were completely different from each filter and methods. These results led us to discard this star from being a possible variable. Figure 12 shows the initial period analysis of the periodograms for each filter in the left-hand panel, while in the right-hand panel it shows the periodogram considering the IRAF PDM discard.

In the case of Star N° 80, the periods that IRAF PDM displayed were $P_V \sim 0.32$ days and $P_I \sim 0.36$ days, while the GLS period was below the limit of the FAP threshold, and the next possible periods for GLS and PDM were different between each filter ($P_V \sim 0.16$ and $P_I \sim 0.11$ days, respectively). The periodogram of this star is shown in Figure 11 (right-hand panel).

Finally, for Star N° 81, the periods that the IRAF PDM analysis displayed were different for each filter, and when revising a new possible period both GLS and PDM gave different results. Other possible periods were below the FAP threshold of the GLS analysis for the $I$ filter. We can also see the differences in the periods in Table 4.

Star N° 41 was initially labeled as a candidate and then the significance test classified it as dubious variable. After revisiting it, we decided to discard this star from being a variable. This was one of those cases where the star, even if it displays a variable behavior when phasing its LC, was discarded as a candidate based on the IRAF PDM analysis and the revised period is too close to the FAP threshold. Its amplitude is also similar to the rms of the data, in a manner similar to Star N° 62. The periodogram for this star is shown in Figure 13.

## 5. Summary and Conclusions

We present in this paper the results of the variability analysis for 510 LC of 255 giant stars in the GC NGC 3201 following up the study made in Albornoz et al. (2021) to find new variable stars for future spectroscopic analysis. To analyze each LC, we performed the GLS and the PDM methods from the PyAstronomy package along with a set of initial discarding

criteria to check for candidate variables. Of the total sample of 255 giant stars, 88 targets were considered as candidates, which were studied in a significance test to be classified as variable, possible, dubious, or non-variable. From this test, 18 targets were classified as variable stars, 29 as either possible or dubious variables, and 41 as non-variable. A cluster membership determination for these stars was then made using proper motion data from Gaia DR3 archives, which reduced our sample to 81 stars. To confirm the classification that had previously been performed, we re-performed the initial period analysis for the variables, possible, and dubious stars, while also complementing it with the PDM method from the IRAF software.

In this work, we increased the sample of new variable stars that were reported by Albornoz et al. (2021), which was based on the discovery of a metal-poor variable star in NGC 6528 (Muñoz et al. 2018) with similar characteristics, i.e., giant stars with a short period and low amplitude. Additionally, we report the discovery of a RR Lyrae ab with a period $P_V = 0.36028 \pm 0.00116$ and amplitude $A(V) = 0.70348 \pm 0.02895$, whose variability has not been studied previously. Finally, we report two ultralow amplitude RR Lyrae stars (Wallace et al. 2019) type c with a period $P_V = 0.37403 \pm 0.00198$ and amplitude $A(V) = 0.02182 \pm 0.00138$ and type ab with a period $P_V = 0.54748 \pm 0.00365$ and amplitude $A(V) = 0.02575 \pm 0.00128$. Both follow the same patterns in the location in the CMD that the RR Lyrae with ultralow amplitude, i.e., they are located in the HB region.

In our sample, we found four patterns. We normalized the LCs of the stars in our study according to their phase and amplitude and later grouped those that presented the same pattern, as shown in Figure 10. We showed that group 1 had a symmetrical LC, while the LC of group 2 is inclined to the left-hand and the LC of group 3 is tilted to the right-hand. Finally, we notice that the group 4 LC is curved, which we classify as W Ursae Majoris stars (contact binaries). To help visualize these patterns, we draw a fit represented by a red line in Figure 10.

Finally, we propose to corroborate the variability of the stars cataloged as possible and dubious variables. This requires more observational data, which will improve the precision in determining these stars.

## Acknowledgments

We extend our gratitude to the anonymous referee for their suggestions and careful review of this manuscript, which undoubtedly contributed to the significant improvement and strengthening of this paper. C.C.C gratefully acknowledges the support provided by MINEDUC ADAIN project TAL2293. S. V. gratefully acknowledges the support provided by Fondecyt reg. No. 1220264. S.V. gratefully acknowledges also the support provided by the ANID BASAL projects ACE210002 and FB210003. This work is based on data acquired at Complejo Astronómico El Leoncito, which is operated under agreement between the Consejo Nacional de Investigaciones Científicas y Técnicas de la República Argentina and the National Universities of La Plata, Córdoba and San Juan. Furthermore, this work made use of the PyAstronomy package collection and we are thankful at the PyA group for answering our doubts regarding their packages.

This work has made use of data from the European Space Agency (ESA) mission Gaia (https://www.cosmos.esa.int/gaia), processed by the Gaia Data Processing and Analysis Consortium (DPAC, https://www.cosmos.esa.int/web/gaia/dpac/consortium). Funding for the DPAC has been provided by national institutions, in particular the institutions participating in the Gaia Multilateral Agreement.

## ORCID iDs

C. C. Cortés https://orcid.org/0000-0002-5003-3762
Á. Llancaqueo Albornoz https://orcid.org/0000-0003-3131-2464
S. Villanova https://orcid.org/0000-0001-6205-1493
J. A. Ahumada https://orcid.org/0000-0002-7091-5025
C. Parisi https://orcid.org/0000-0001-9382-3986

## References

Albornoz, Á. L., Villanova, S., Cortés, C. C., Ahumada, J. A., & Parisi, C. 2021, AJ, 161, 76
Arellano Ferro, A., Ahumada, J. A., Calderón, J. H., & Kains, N. 2014, RMxAA, 50, 307
Blažko, S. 1907, AN, 175, 325
Bramich, D. M. 2008, MNRAS, 386, L77
Bramich, D. M., Figuera Jaimes, R., Giridhar, S., & Arellano Ferro, A. 2011, MNRAS, 413, 1275
Bramich, D. M., & Freudling, W. 2012, MNRAS, 424, 1584
Bramich, D. M., Horne, K., Albrow, M. D., et al. 2013, MNRAS, 428, 2275
Carretta, E., Bragaglia, A., Gratton, R., & Lucatello, S. 2009a, A&A, 505, 139
Carretta, E., Bragaglia, A., Gratton, R. G., et al. 2009b, A&A, 505, 117
Clement, C. M., Muzzin, A., Dufton, Q., et al. 2001, AJ, 122, 2587
Czesla, S., Schröter, S., Schneider, C. P., et al. 2019, PyA: Python astronomy-related packages, Astrophysics Source Code Library, ascl:1906.010
Eggen, O. J. 1973, ApJ, 184, 793
Eggen, O. J. 1977, ApJ, 213, 767
Gaia Collaboration, Prusti, T., de Bruijne, J. H. J., et al. 2016, A&A, 595, A1
Gaia Collaboration, Vallenari, A., Brown, A. G. A, et al. 2023, A&A, 674, A1
Gonzalez, G., & Wallerstein, G. 1998, AJ, 116, 765
Gratton, R., Sneden, C., & Carretta, E. 2004, ARA&A, 42, 385
Harris, W. E. 1996, AJ, 112, 1487
Kaluzny, J., Rozyczka, M., Thompson, I. B., et al. 2016, AcA, 66, 31
Landolt, A. U. 1992, AJ, 104, 340
Layden, A. C., & Sarajedini, A. 2003, AJ, 125, 208
Lomb, N. R. 1976, Ap&SS, 39, 447
Minniti, D., Lucas, P. W., Emerson, J. P., et al. 2010, NewA, 15, 433
Mucciarelli, A., Lapenna, E., Massari, D., Ferraro, F. R., & Lanzoni, B. 2015, ApJ, 801, 69
Muñoz, C., Geisler, D., & Villanova, S. 2013, MNRAS, 433, 2006
Muñoz, C., Geisler, D., Villanova, S., et al. 2018, A&A, 620, A96
Saito, R. K., Hempel, M., Minniti, D., et al. 2012, A&A, 537, A107
Scargle, J. D. 1982, ApJ, 263, 835
Simmerer, J., Ivans, I. I., Filler, D., et al. 2013, ApJL, 764, L7
Stellingwerf, R. F. 1978, ApJ, 224, 953
Stetson, P. B. 2000, PASP, 112, 925
Taylor, M. B. 2005, in ASP Conf. Ser. 347, Astronomical Data Analysis Software and Systems XIV, ed. P. Shopbell, M. Britton, & R. Ebert (San Francisco, CA: ASP), 29
Tody, D. 1986, Proc. SPIE, 627, 733
Villanova, S., Geisler, D., Carraro, G., Moni Bidin, C., & Muñoz, C. 2013, ApJ, 778, 186
Wallace, J. J., Hartman, J. D., Bakos, G. Á., & Bhatti, W. 2019, ApJL, 870, L7
Zechmeister, M., & Kürster, M. 2009, A&A, 496, 577